Improved Electric Wiring of Hemoglobin with Impure-Multiwalled Carbon Nanotube/Nafion Modified Glassy Carbon Electrode and Its Highly Selective Hydrogen Peroxide Biosensing

ARTICLE *in* THE JOURNAL OF PHYSICAL CHEMISTRY C · OCTOBER 2012

Impact Factor: 4.77 · DOI: 10.1021/jp3064933

4 AUTHORS:

Annamalai Senthil Kumar
VIT University
129 PUBLICATIONS **2,169** CITATIONS
SEE PROFILE

Gayathri Prakasam
VIT University
8 PUBLICATIONS **73** CITATIONS
SEE PROFILE

Barathi Devaraj
VIT University
13 PUBLICATIONS **106** CITATIONS
SEE PROFILE

Rajagopalan Vijayaraghavan
VIT University
26 PUBLICATIONS **411** CITATIONS
SEE PROFILE

THE JOURNAL OF PHYSICAL CHEMISTRY C

Article

pubs.acs.org/JPCC

Improved Electric Wiring of Hemoglobin with Impure-Multiwalled Carbon Nanotube/Nafion Modified Glassy Carbon Electrode and Its Highly Selective Hydrogen Peroxide Biosensing

Annamalai Senthil Kumar,*[,†] Prakasam Gayathri,[†] Palani Barathi,[†] and Rajagopalan Vijayaraghavan[‡]

[†]Environmental and Analytical Chemistry Division, School of Advanced Sciences, Vellore Institute of Technology University, Vellore-632014, India

[‡]Material Chemistry Division, School of Advanced Sciences, Vellore Institute of Technology University, Vellore-632014, India

Supporting Information

ABSTRACT: A hemoglobin (Hb) modified glassy carbon electrode consisting of low cost as commercially received impure-multiwalled carbon nanotube (i-MWCNT, 90% purity) and nafion (GCE/i-MWCNT@Hb/Nf) has been demonstrated for improved electric wiring of Hb and efficient direct electron-transfer characteristics. This report is the first attempt for coupling i-MWCNT with Hb for the biosensor purpose. The Hb electrode was assembled by a simple preparation procedure within 38.3 (±2.5) min of time, without any linker, surfactant, promoters, and extensive functionalization of the MWCNT. Impurities within the i-MWCNT such as metal oxides (Fe_3O_4, Co_3O_4, and NiO), graphite, and amorphous carbon were quantitatively identified by X-ray diffraction (XRD) and thermogravimetric analysis (TGA). The metal oxide impurities were found to assist the binding of Hb onto i-MWCNT, whereas the graphitic impurity facilitated the direct electron-transfer reaction. The measured surface excess value of the Hb on the GCE/CNT@Hb/Nf with respect to different CNTs are in the sequences of i-MWCNT > purified-MWCNT > impure single-walled carbon nanotube > functionalized-MWCNT. The GCE/i-MWCNT@Hb/Nf shows enhanced and selective H_2O_2 electrocatalytic reduction signal without interference from cysteine, ascorbic acid, uric acid, nitrite, and nitrate. Note that Hb can mediate the nitrite reduction reaction too; however, no interference has been observed in this work. Various types of milk, cosmetic bleaching cream, and medical real samples were successfully analyzed with recovery values closer to 100%. The electrode has been found to be stable for 110 days.

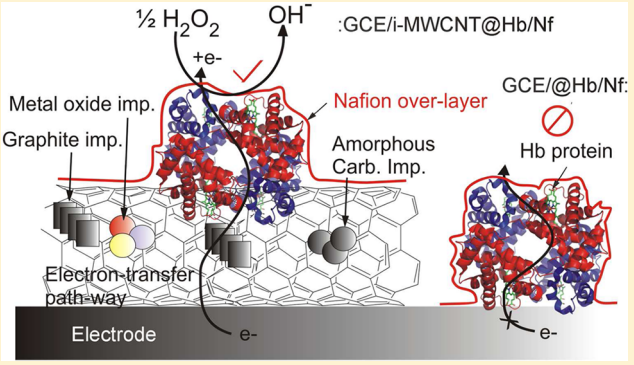

1. INTRODUCTION

The study of direct electrochemistry of redox enzymes not only provides a working model to examine the mechanism of electron transfer reactions of enzymes in biological systems[1] but also establishes a platform for fabricating new kinds of biofuel system,[2] biosensors,[3] enzymatic bioreactors,[4] and biomedical devices[5] that do not use any mediators and promoters. Hemoglobin (Hb, molecular weight of 64.5 kD) is the iron-containing oxygen-transport metalloprotein in the red blood cells of all vertebrates.[6] Hb does not play a role as an electron carrier in biological systems.[6] However, it has been shown to possess enzymelike catalytic activity.[1] It is also an ideal model molecule for the study of direct electron transfer reactions of enzymes because of its known and documented structure.[1,6] The electron transfer between the Hb and conventional solid electrodes viz., glassy carbon (GCE), platinum, and gold are very slow and often results in loss of both electrochemical and bioactivity; possibly due to inaccessibility of the buried prosthetic heme active sites and bioincompatibility respectively. Efforts have been made by combining the Hb with surfactant[7−10] and redox mediators like toluidine blue,[11] riboflavin,[12] poly(Nile Blue),[13] methylene blue,[14] rhein,[15] and ferrocene carboxylic acid,[16] to turn the Hb electron-transfer characteristics. However, direct electron transfer behavior of the Hb was achieved on the surface of some special materials such as TiO_2 nanotubes,[17] nanocrystalline SnO_2,[18] mesoporous Al_2O_3,[19] CdS/Mn,[20] CuO nanowire bundles,[21] clay,[22] lipid protected gold nanoparticles[23] and colloidal silver nanoparticles/chitosan,[24] carbon nanotube (CNT)/cetyl trimethylammonium bromide (CTAB),[25] and CNT graphene/Pt nanoparticle composites.[26] Among them, CNT and graphene are of special interest due to their unique structures, very high conducting, good mechanical, and biocompatible properties.

In 2004, Cai et al and Yang et al groups first demonstrated the direct electrochemistry of the Hb on a GCE modified with

Received: July 1, 2012
Revised: October 12, 2012
Published: October 17, 2012

   dx.doi.org/10.1021/jp3064933 | J. Phys. Chem. C 2012, 116, 23692−23703

acid-treated CNT and cationic surfactant, CTAB, or dodecyl-*N*,*N*-dimethyl-1-dodecanaminium bromide (DDDB) systems, independently.[25,27] In the electrode preparation, a mixture consisting of 1 mg/mL CNT + 1% CTAB + 5 mg/mL of Hb was coated on a GCE and subsequently protected by a nafion (Nf) membrane. Meanwhile, in 2006, a Hb+acid treated-MWCNT mixture modified pyrolytic graphite electrode (surface excess, $\Gamma_{Hb} = 3.1\times 10^{-11}$ mol/cm^2) was also reported for the direct electron-transfer behavior.[28] Main purpose of the acid treatment of the CNT is to generate oxygen rich surface functional groups (designated as f-CNT, *f* = functionalized), which are hydrophilic in nature, and to effectively bind the Hb protein through the following methods: (i) hydrophilic−hydrophilic interaction between the f-CNT and protein units of the Hb, and (ii) covalent or electrostatic bonding of Hb's amino groups with the carbonyl functional group of the f-CNT. Unfortunately, the Hb modified CNT systems showed feeble redox behavior with very low Γ_{Hb} value of 0.01×10^{-10} mol/cm^2.[25] To increase the Γ_{Hb} value, functionalized-CNT mixed with promoters and organic linkers such as sodium dodecyl sulfate (SDS) surfactant combined gold colloidal nanoparticles,[29] positively charged gold/pyridine derivative nanoparticles,[30] 3-dimethylaminopropyl carbodiimide (EDC),[31] cerium dioxide/chitosan composite,[32] ionic liquid,[33] poly(ethylene glycol) grafted units,[34] and hydroxyapatite[35] systems have been used. A Γ_{Hb} value in the range $47—52 \times 10^{-10}$ mol/cm^2 could be achieved along with an apparent electron-transfer rate constant value in between 0.05 to 0.99/s.[31,33] Even though the above CNT composites could give high Γ_{Hb} values, the preparation methods for the Hb modified electrodes are time consuming and involved with several synthetic steps.[33,36] Meanwhile, successive bulk electrochemical deposition method of Hb-f-CNT-nafion layer ($\Gamma_{Hb} = 1.7 \times 10^{-10}$ mol/cm^2) on a GCE in a diluted sulfuric acid bath condition was also reported recently.[36]

Here in, we are reporting a simple preparation method for enhanced electric wiring of Hb on an impure-MWCNT (i-MWCNT, *i* = impure) modified GCE (designated as GCE/i-MWCNT@Hb) without any linkers, composite materials, acid preparation bath, and bulk deposition methods. Indeed, we have improved the Cai et al's electrode preparation procedure[25] by replacing the strong acid treated functionalized CNT, that is, f-CNT to as commercially received low cost i-MWCNT (purity ∼90% on carbon basis) and with a different way of coating technique. Hydrogen peroxide (H_2O_2) reduction reaction was taken as a model system to study the Hb behavior of the newly prepared GCE/i-MWCNT@Hb. Note that influence of the trace internal impurities such as carbonaceous, amorphous carbon, and nanometallic oxides like Fe, Co, and Ni, which are encapsulated or staged inside the CNTs, on the electron-transfer behavior of CNT were already explored.[36] In 2006, Compton group pointed out that the nanoiron impurity of CNT was responsible for the H_2O_2 electrocatalytic reaction for the first time.[37a,b] Later, Pumera and his co-workers made extensive studies on the different types of *trace* impurities for specific electrochemical behaviors of the CNTs.[37c,d] For instance, CNT's impurity, viz., trace nano-Fe/Co/Ni oxides for hydrazine mediation,[37e] nanographite parts for enhanced electron-transfer behavior of $Fe^{III}(CN)_6^{3-}/Fe^{II}(CN)_6^{4-}$ redox couple,[37f] and oxidations of tyrosine, tryptophan, *β*-nicotinamide adenine dinucleotide,[37g] phenol,[37h] insulin, nitric oxide and thiols,[37i] and amorphous carbon traces for the enhancement of $Fe^{III}(CN)_6^{3-}/Fe^{II}(CN)_6^{4-}$ redox behavior.[37j] In this work, graphitic carbon impurity within i-MWCNT was found to be key for the enhanced direct electron-transfer function and nano-Fe/Co/Ni oxide impurities attributed for the strong binding of Hb protein on the i-MWCNT surface. Overall, the i-MWCNT@Hb modified electrode shows efficient electron-transfer, higher surface active Hb sites, that is, Γ_{Hb}, selective and sensitive electrocatalytic response to H_2O_2 reduction reaction in neutral pH, in this work. Finally, quantitative detection of H_2O_2 contents in different milks, cosmetic and medical real samples using the new electrode was successfully demonstrated.

2. EXPERIMENTAL SECTION

2.1. Reagents and Materials. Human Hb, impure MWCNT (i-MWCNT, ∼90% purity on carbon basis, size 7−15 nm × 0.5−10 *μ*m), impure single-walled carbon nanotube (i-SWCNT, ∼70% purity on carbon basis, size 0.7−1.1 nm diameter), nickel(II) oxide nanopowder of size 50 nm (99.8% trace metal basis), and iron(II,III) oxide nanopowder of size 50 nm (∼98% trace metal basis) were purchased from Aldrich (USA). Cobalt oxide powder was supplied from SD fine (India). Graphite nanopowder (400 nm, ∼98% purity) was obtained from SRL (India). Hydrogen peroxide (30%) was received from Rankem (India) and stored in refrigerator. Other chemicals were of analytical grade and used as received without further purification. Aqueous solutions were prepared using deionized and alkaline $KMnO_4$ distilled water (designated as DD water). Unless otherwise stated, 20 min N_2 purged pH 7 phosphate buffer solution (PBS) of ionic strength 0.1 M was used as a supporting electrolyte.

2.2. Apparatus. Electrochemical measurements were carried out using CHI model 660C electrochemical workstation, USA, with 10 mL working volume. The three electrode system consisted of GCE of 0.0707 cm^2 geometrical surface area and its chemically modified form (CME) as a working electrode, Ag/AgCl with 3 M KCl as a reference electrode, and platinum wire as a counter electrode. The Bioanalytical system (BAS, USA) polishing kit was used to polish the GCE surface. The surface of the GCE was cleaned both mechanically and electrochemically by polishing with 0.5 *μ*m alumina powder, washing with DD water, and sonicating for 5 min followed by performing cyclic voltammetry (CV) for 10 cycles in the potential window −0.2 to 1 V versus Ag/AgCl at a potential scan rate (*v*) of 50 mV/s in pH 7 PBS. Electrochemical quartz crystal microbalance (EQCM) experiments were performed using CHI 440B workstation along with Gold-EQCM (Au-EQCM, 0.19 cm^2) electrode as a working system. Before the CME preparation, the Au-EQCM electrode was thoroughly washed with acetone, DD water and electrochemically pretreated as per the procedure mentioned above. Surface characterizations of the Hb protein modified working electrodes were done with a field emission scanning electron microscope instrument (FESEM, Hitachi SU6600). Nanosurf Easyscan 2, Switzerland, atomic force microscope (AFM) instrument was also used for the surface morphology analysis. Thermal stability experiments were carried out using Simultaneous DSC-TGA, TA Instruments SDT Q600, USA with ultrapure Oxygen atmosphere at 4 °C per minute up to 1000 °C. A Bruker D8 Advanced diffractometer X-ray diffraction (XRD, Germany) instrument with a Cu K*α* source (*λ* = 1.5418 A°) was used to analyze the phases present in carbon materials.

2.3. Procedures. Purified and functionalized MWCNT (i.e., p-MWCNT and f-MWCNT, where *p* = purified) were

dx.doi.org/10.1021/jp3064933 | J. Phys. Chem. C 2012, 116, 23692−23703

Scheme 1. Illustration for the GCE/i-MWCNT@Hb/Nf Electrode Preparation and Its Selective Electrocatalytic H_2O_2 Reduction Function

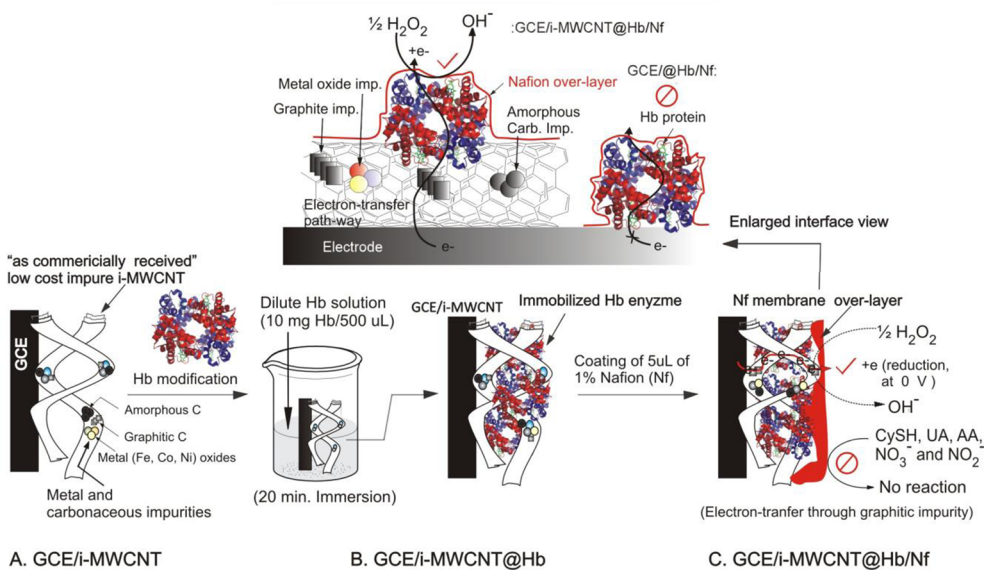

Table 1. TGA Results of Various Carbon Samples[a]

		Species (%)				
	carbon samples	ads. H_2O (<180 °C)	amp. carbon-imp (~180–300 °C)	CNT unit (~300–500 °C)	graphite-imp. (~770 °C)	metal oxide-imp. (~770–1000 °C)
1	i-MWCNT	1.1	1.2 (ca.)	92.1	0.48	5.2
2.	p-MWCNT	0.3	NM	90.5	DM	DM
3.	f-MWCNT	3.5	NM	94.2	NM	2.2 (ca.)
4.	i-SWCNT	2.2	4.8	66.5	2.07	24.4 (ca.)
5.	graphite	0.4%	NM	95.9		3.7 (ca.)

[a]NM: not measurable (considered to be ~0%); DM: Difficulty in measuring (positive increase in the mass (weight gain) response noticed, may be metallic impurities can take up oxygen); ca: calculated based on the other available data by subtracting from total 100%.

prepared as per our previous reported procedures,[38,39] where the mixture of 200 mg of i-MWCNTs + 35 mL of 6 M (dilute) or 15 M HNO_3 (fuming acid) was refluxed for 12 h in a silicone oil bath at T = 413(±2) K (140 °C), filtered, washed with copious amount of DD H_2O until the pH of the filterant solution become neutral, and finally dried at T = 353 (±2) K (80 °C) in a vacuum oven. The fuming HNO_3 treatment results to generation of rich carboxylic acid (−COOH) functional group.[40]

For the GCE/CNT@Hb preparation, first, 5 μL of the respective CNT/ethanol suspension (1 mg/500 μL ethanol) was drop coated on a clean GCE and kept for drying in room temperature (298 ± 2 K or 25 ± 2 °C) for 2(±0.5) min. The GCE/CNT modified electrode was then electrochemically pretreated by continuous cycling (n = 10, n = no. of cycles) in the potential window −0.5 to 0.5 V versus Ag/AgCl in pH 7 PBS at v = 50 mV/s (3.3 min). Hb stock solution was prepared by dissolving 10 mg of Hb solid in 500 μL pH 7 PBS and stored for a week in RT (optimal). The Hb protein was finally immobilized on the GCE/CNT by immersion method, in which the GCE/CNT was dipped in the Hb stock solution for 20(±1) min, washed, and again dried in air. Finally, 5 μL of 1% nafion-ethanolic solution was casted on the surface and dried for 5(±1) min in room temperature. All other control Hb CMEs were prepared in a similar way to above case with 1 mg/500 μL ethanol of carbon and other metal oxide materials. Prior to the electrochemical experiments, the freshly prepared CNT@Hb electrodes (GCE/CNT@Hb/Nf) were pretreated in the potential window of −0.7 to 0.5 V versus Ag/AgCl in pH 7 PBS for 20 continuous cycles at v = 50 mV/s (8 min). Scheme 1 illustrates overall information for the preparation of the GCE/i-MWCNT@Hb/Nf (optimal). Note that a total time of 38.3(±2.5) min only is required for the preparation of the optimal working electrode.

2.4. Real Sample Analyses. Two pasteurized milk samples (Aavin milk #1, and Shruthi milk #2) purchased from a local milk shop, a cosmetic fairness bleach cream (Fem, India #3) obtained from local departmental store and a medical hydrogen peroxide solution (#4, no details for the H_2O_2 concentration) collected from the VIT university health care center, were subjected to real sample analyses. All of the samples were stored in refrigerator until use. There was no display about the H_2O_2 content in the labels of the real samples. For the real sample #3 preparation, 1 g of the bleach cream sample mixed with 10 mL of pH 7 PBS, sonicated, and filtered was used. In the case of medical real sample #4 preparation, 100 μL of sample was mixed with 9.9 mL of pH 7 PBS. However, for the milk #1 and #2 preparations, the raw samples were directly subjected for the real sample analysis after adding with suitable buffer salts. Real sample analyses were carried out using amperometric i–t method with 10 (#1) or 20 (#2) or 50 μL (#3 and #4) spikes of the analyte into the 10 mL electrochemical bath.

dx.doi.org/10.1021/jp3064933 | J. Phys. Chem. C 2012, 116, 23692–23703

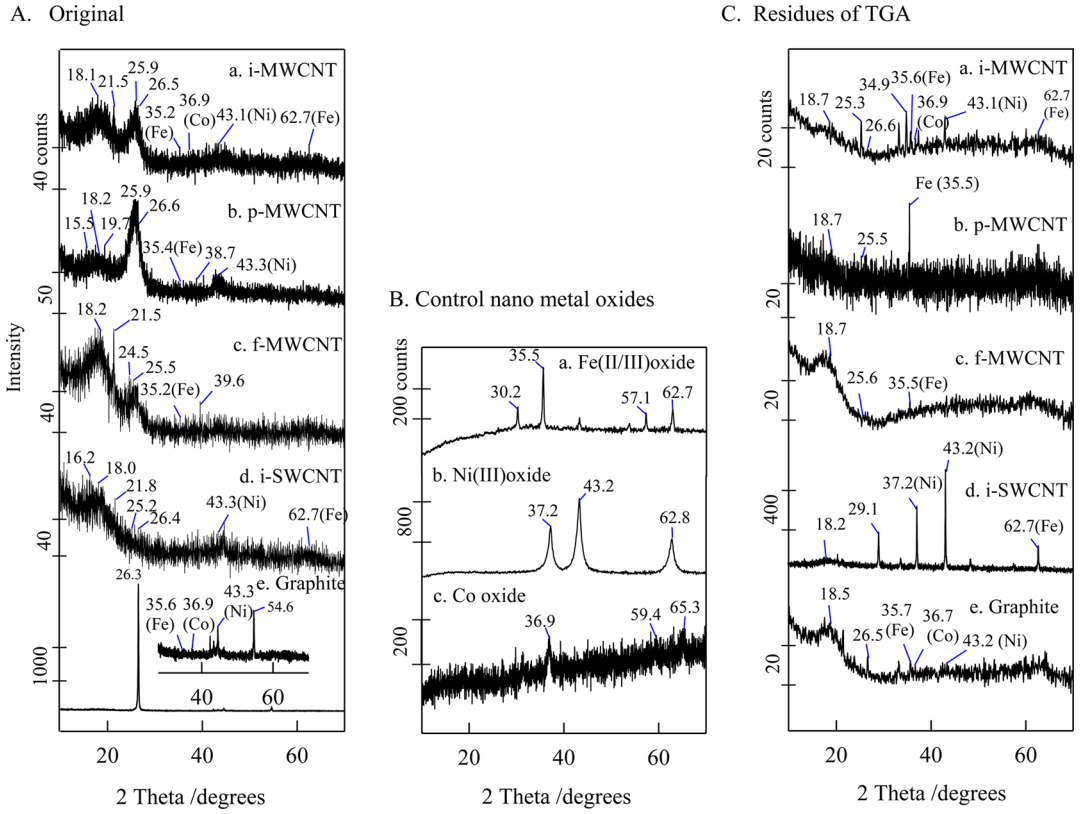

Figure 1. Typical XRD patterns of (A) various carbon and (B) metal oxide materials. (C) XRD results of the TGA residues.

3. RESULTS AND DISCUSSION

3.1. Thermal and XRD Characterizations of the Different CNTs. To estimate the amounts of impurities quantitatively in various samples, TGA and XRD were employed in complementary fashion. The phases present in the sample before and after TGA run (O_2 atm. heating rate up to 1000 °C) were quantitatively analyzed. TGA in O_2 atmosphere would burn the combustible carbon and the residue analyzed by XRD would give noncombustible carbon and metal oxide/s.[41a] Hence, the combination of the two would reveal the presence of various impurities such as oxides of Ni, Fe, Co, and C samples. First, discrete TGA of i-MWCNT, p-MWCNT, f-MWCNT, i-SWCNT, and nanographite powder samples were done and the results were displayed in parts A−E of Figure S1 of the Supporting Information. Obtained TGA profiles of the samples are qualitatively same. Initially, plateau-like region with feeble change in the weight% up to ∼400 °C was noticed. However, in the temperature range 400−600 °C, significant weight loss occurred. From 600 to 1000 °C, there is no weight loss after that nearly unaltered line-like responses were noticed. Table 1 provide quantitative TGA data for the different molecules viz., adsorbed H_2O (<180 °C),[41a,b] amorphous carbon impurity (∼400 °C),[41b] CNT unit (∼500 °C),[41c] graphite (∼550−750 °C, both as impurity and control),[41d] and metal oxide (∼770−1000 °C)[41a] impurities based on their respective specific weight loss peaks at different temperature regions. The following information can be drawn from the output data: (i) order of the decomposition temperature with respect to the maxima DTGA peak for the different carbons is, i-SWCNT (391 °C) < i-MWCNT (546 °C) < f-MWCNT ≅ p-MWCNT (565 °C) < graphite (682 °C). Presumably, metal impurities and oxygen-functional groups might have assisted the early decomposition of the sp^2 carbon in CNT (parts A and C of Figure S1 of the Supporting Information); (ii) even after the mild (for p-MWCNT) or strong (for f-MWCNT) acid purification the i-MWCNT did not result in complete removal of the impurities, especially metal oxide traces were not removed (Table 1). This observation is parallel with Pumera's report for incomplete removal of the impurities from CNTs.[41e] Thus, characterization by inductive coupled plasma-Mass analysis (ICP-MS), where concentric acid based sample preparation method being used, could not support precise information about the impurity levels; (iii) order of the carbons with respect to total metal oxide impurity viz., i-SWCNT(24.4%) > i-MWCNT (5.2%) > f-MWCNT (2.2%); (iv) graphite impurity was identified in support with a control graphite powder, and its percent weight loss compared with i-MWCNT and i-SWCNT samples are 0.48 and 2.07, respectively (Figure S1 of the Supporting Information and Table 1). There was a difficulty in measuring graphitic and metallic impurities with p-MWCNT due to some weight gain (possibly fraction of impure metal/s become metal oxides, insert plot in part B of Figure S1 of the Supporting Information); (v) f-MWCNT failed to show any measurable graphite impurity (Table 1); (vi) amorphous carbon impurity was identified only with i-SWCNT (4.8%) and i-MWCNT (1.2%) samples (Figure S1 and Table 1). Meanwhile, discrete XRD patterns of different CNTs and control graphite samples showed specific peaks corresponding to sp^2 hexagon carbon units ($2\theta \cong 25.9°$),[38] graphitic carbon ($2\theta \cong 26.3°$),[41d] carboxylic functionalized carbon ($2\theta \cong 18.1°$),[41d] and impurities of Iron oxide (Fe_3O_4; $2\theta \cong 35.5$, 30.2, 62.7, and 57.1°),[41f] Ni oxide (NiO; $2\theta \cong 43.2$, 37.2, and 62.8°)[41g] and Co oxide (Co_3O_4; $2\theta \cong 36.9$, 65.3, and 59.4°)[41f] (part A of Figure 1). The i-SWCNT sample does not possess cobalt oxide peak

dx.doi.org/10.1021/jp3064933 | J. Phys. Chem. C 2012, 116, 23692−23703

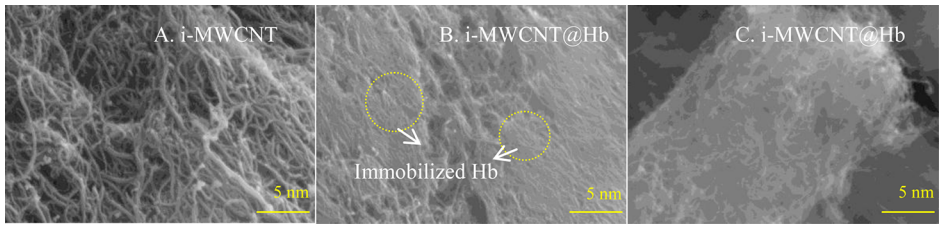

Figure 2. SEM images of the (A) unmodified i-MWCNT and (B and C) i-MWCNT@Hb hybrid materials.

(d in part A of Figure 1) as revealed by XRD. Control metal oxides were also analyzed by XRD, as in part B of Figure 1, to confirm their presence and absence. Note that graphite carbon also showed traces of impurities corresponds to iron, nickel, and cobalt oxides (e in part A of Figure 1 and Table S1 of the Supporting Information).

XRD patterns of the TGA residues (char yields) are displayed in part C of Figure 1. Corresponding 2θ values and possible species are summarized in Table S1 of the Supporting Information. This analysis can provide precise quantitative amounts of metal oxide impurities present in the various samples as there are stable even at 1000 °C, which is the maximum temperature of TGA run. However, for the carbon, becaues it can be burned out (>90%) at early temperatures (~500 °C), this technique would not support any useful information. It is interesting to see marked and multiple XRD peaks with the TGA residue of i-MWCNT sample, which are due to metal oxide impurities of Fe, Ni, and Co (Table S1 of the Supporting Information). This observation is true with the TGA residues of p-MWCNT, f-MWCNT (intense response), i-SWCNT (absence of Co_3O_4), and graphite samples too. Note that only with the p-MWCNT and f-MWCNT residues characteristic iron oxide peak was noticed (2θ = 35.5°). The following conclusions can be drawn from the XRD/TGA residue analyses: (i) the commercially purchased i-SWCNT, i-MWCNT, and graphite samples have oxides of iron, nickel, and cobalt oxide as impurities and (ii) acid washing of i-MWCNT can remove nickel and cobalt oxide impurities; not iron oxide. Iron oxide impurities are still retained with p-MWCNT and f-MWCNT samples.

3.2. Physicochemical Characterizations of Hb Modified Systems. Morphology of the Hb modified i-MWCNT surface, that is, i-MWCNT@Hb was examined by SEM. Since the nafion overlayer can hinder to view the i-MWCNT/Hb in the i-MWCNT@Hb/Nf system (optimal); we have neglected the nafion layer in the SEM characterization. Parts A–C of Figure 2 show SEM photographs of i-MWCNT and i-MWCNT@Hb. A coil-like structure of i-MWCNT is seen in part A of Figure 2. Part C of Figure 2 is a magnified view of one of the coil-like structures obtained from i-MWCNT@Hb. After the Hb modification, a nearly uniform and smooth surface was noticed (part B of Figure 2), which might be due to the entrapment of the Hb in the vacant space between the i-MWCNT coil structure. Meanwhile, AFM characterization results for the i-MWCNT@Hb and i-MWCNT films were displayed in Figure S2 of the Supporting Information. Because of practical difficulty, 0.5% nafion being used as a medium to disperse i-MWCNT. The Hb immobilized layer showed islands-like structure, dimension ~3 μm, on the optimal electrode. However, the morphology ensures immobilization of the Hb on the GCE/i-MWCNT@Hb electrode surface. Presumably, the i-MWCNT modified electrode behaves as a spongelike material and can uptake the significant amount of the Hb within the coil structure. If nafion is coated as over layer on the i-MWCN@Hb, it will protect and seal the entire CME.

Stability and compatibility of the Hb protein/CNT within the optimal CME was tested using FTIR spectroscopy. For the case of nondenatured protein, characteristic IR bands at 1700–1600 cm^{-1} and 1620–1500 cm^{-1} respectively due to the carbonyl functional group stretching (amide-I) and N–H bending/C–N stretching (amide-II) vibrations of the backbone of Hb protein will be present.[42a] However, if Hb is denatured, the sharpness and position of the Amide-I and II bands will be altered or even absent.[42b] Part A of Figure 3 is comparative KBr/FT-IR patterns of Nf, i-MWCNT, Hb, and i-MWCN@Hb/Nf systems. For the analysis, the respective GCE-CME was

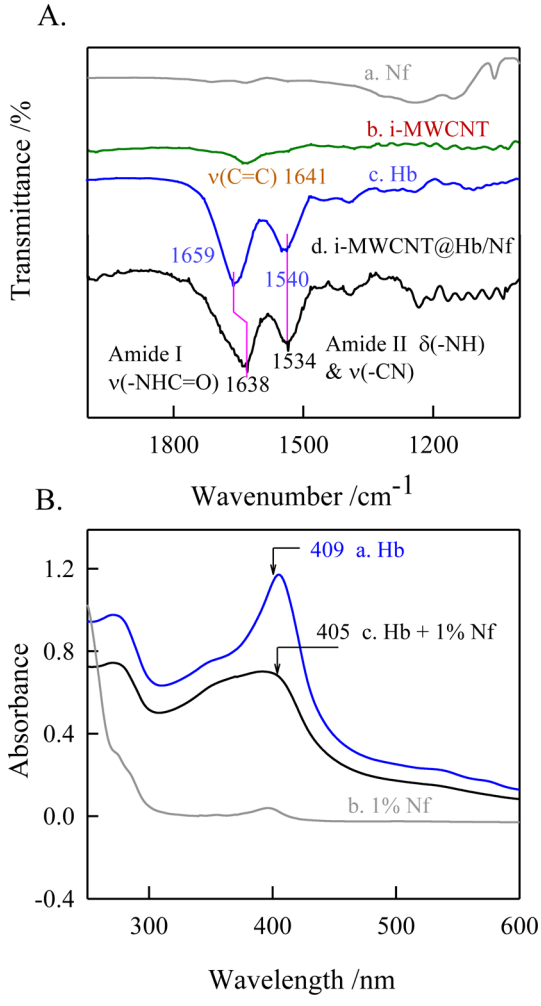

Figure 3. (A) Typical FTIR pattern of i-MWCNT@Hb/Nf in addition with its control samples; (B) UV–vis response of dilute Nf, Hb, and Nf + Hb systems.

dx.doi.org/10.1021/jp3064933 | J. Phys. Chem. C 2012, 116, 23692–23703

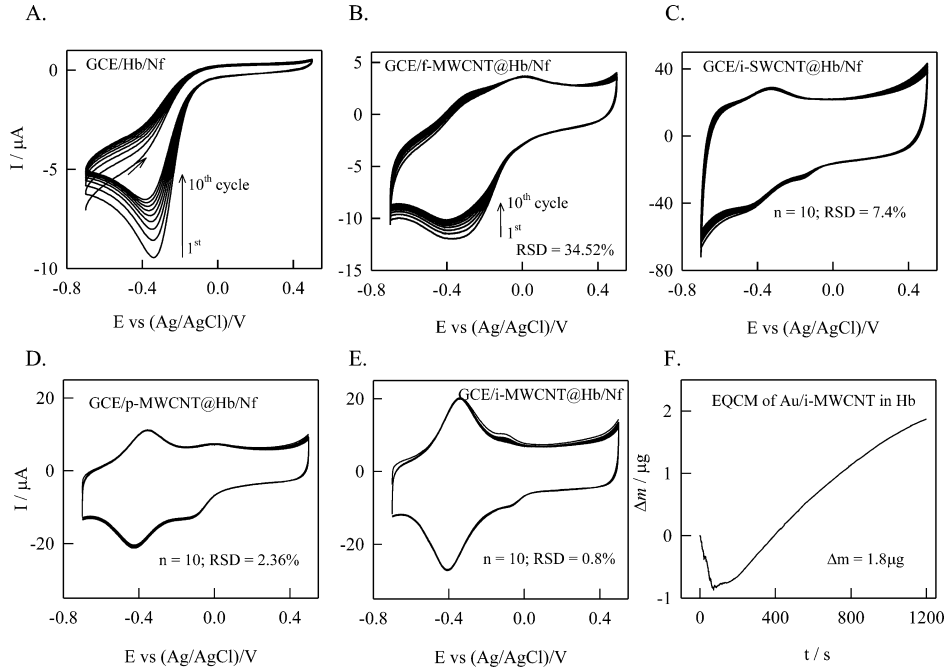

Figure 4. Ten continuous cyclic voltammetric responses of (A) GCE/Hb/Nf, (B) GCE/f-MWCNT@Hb/Nf (f = functionalized), (C) GCE/i-SWCNT@Hb/Nf, (D) GCE/p-MWCNT@Hb/Nf (p = purified), and (E) GCE/i-MWCNT@Hb/Nf in pH 7 PBS at a scan rate of 50 mV/s; (F) open circuit EQCM response of a Au/i-MWCNT electrode with 10 mg Hb dissolved 500 μL pH 7 PBS.

scratched out and subjected to KBr/FTIR experiment. Hb protein showed FTIR bands at 1659 and 1540 cm^{-1} and for i-MWCNT@Hb/Nf the values appeared at 1638 and 1534 cm^{-1}. The slight shift, that is, 21 and 6 cm^{-1} observed with the above FTIR signals may be due interaction of the hydrophobic and hydrophilic functional groups of the Hb with the MWCNT/Nf system. Nafion is a highly stable and rigid perfluoro polymeric proton/cationic exchanging membrane containing specific hydrophobic ($-CF_2-CF_2$) and hydrophilic ($-SO_3H^+$) micro-channels,[43] and it is expected that these channels along with hydrophobic sites of MWCNT, that is, the basal plane can interact with Hb and could stabilize the sandwiched Hb structure, that is i-MWCNT@Hb/Nf. To further support the expectation, Hb and nafion samples were subjected to UV−vis analysis (part B of Figure 3). Because the i-MWCNT layer has solid thin-film-like structure (underlying) and is opaque in nature, we could not extend it to UV−vis studies. As can be seen in the figure, a specific UV−vis signal at λ_{max} = 409 nm, due to the Soret absorption band of the Heme group, was altered upon addition of 1% of nafion−ethanol solution (λ_{max} = 405 nm).[42b] The observation speculates some positive interaction between Hb and nafion and Hb conformation change in the optimal working electrode.[42a] Later, stability investigation by cyclic voltammetry showed over 100 days stability of room temperature (298 K) preserved screen-printed carbon electrode (SPCE)/i-MWCNT@Hb/Nf system (section 3.7), which further support the speculation.

3.3. Direct Electrochemistry of the GCE/CNT@Hb/Nf Film. Control CV response of a Hb modified nafion overlayer coated GCE (GCE/Hb/Nf) in pH 7 PBS is displayed in part A of Figure 4. An unstable and irreversible ($i_{pc}/i_{pa} \gg 1$, i_{pc} = cathodic peak, and i_{pa} = anodic peak currents) reduction peak appeared at −0.38(±0.03) V versus Ag/AgCl corresponds to the reduction of the Hb-heme Fe(III)/Fe(II) sites. The instability behavior of the CV peak currents indicates denaturation or decomposition of the Hb. This observation concludes the bioincompatibility of the GCE/Hb/Nf matrix system for the stable and direct electron-transfer behavior of the Hb. In the next step, GCE/f-MWCNT@Hb/Nf, where the f-MWCNT = carboxyl functionalized MWCNT, was subjected for the CV examination. As can be seen in part B of Figure 4, a broad and irreversible peak at −0.38(±0.05) V was observed along with large background current signal. It has been reported that the f-CNT with a surface group like carboxylic acid can electrostatically interact with positive charged sites of protein (Hb) and thereby strongly attached on the surface.[25,27] However, for the electron tunnelling between f-CNT and Hb, an additional promotor or linker such as CTAB, SDS, EDC, and gold nanoparticles is needed to facilitate the electron-transfer reaction.[29−35] In the present case, because the f-MWCNT was attached directly with Hb without any promotor or mediator, the composite electrode structure did not promote the Hb-Fe(III)/Fe(II) electron-transfer behavior reversibly. Regarding the irreversible observation, it is expected that the anionic polymeric membrane nafion, which has been coated on the f-MWCNT@Hb might have altered the Hb-protein's microenvironment and in turn bioincompatible in nature. Meanwhile, single walled carbon nanotube (i-SWCNT)-Hb-Nf modified electrode, GCE/i-SWCNT@Hb/Nf was also examined for the suitability (part C of Figure 4). Interestingly, unlike to the previous cases, the i-SWCNT@Hb/Nf system shows a feeble redox peak at an apparent standard electrode potential, $E^{o\prime} = (E_{pc} + E_{pa})/2$ and the Γ_{Hb} values are −0.38(±0.01) V versus Ag/AgCl and 9.6 (±0.2) × 10^{-10} mol/cm^2, respectively. Relative standard deviation (RSD) of 10 continuous CV cycles of the Hb electrode is 7.4%. Extended experiments with (p-MWCNT)-Hb-Nf modified electrode, GCE/p-MWCNT@Hb/Nf yielded well-defined redox behavior with $E^{o\prime}$ and Γ_{Hb} values of −0.38(±0.01) V versus Ag/AgCl and 29.05(±2.1) × 10^{-10} mol/cm^2, respectively (part D of Figure 4). Note that the Γ_{Hb} value is 3 times higher than the GCE/i-SWCNT@Hb/Nf's value, which reveals larger uptake of the Hb by the p-MWCNT

dx.doi.org/10.1021/jp3064933 | J. Phys. Chem. C 2012, 116, 23692−23703

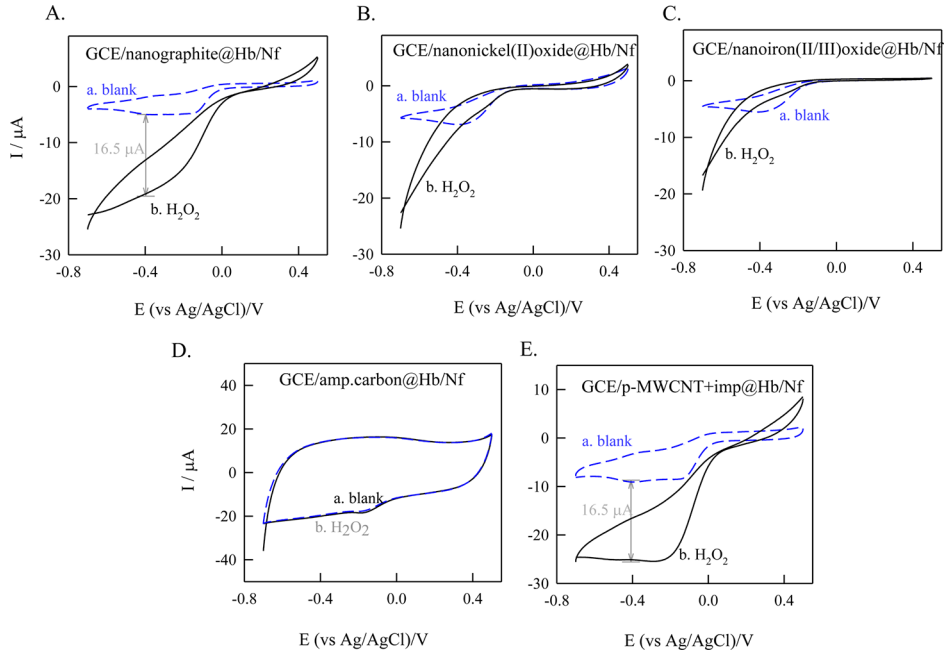

Figure 5. CV responses of several control electrodes; (A) nanographite, (B) nanonickel(II) oxide, (C) nanoiron(II/III) oxide, and (D) amorphous carbon chemically modified with Hb and nafion without and with 500 μM H_2O_2. (E) CV of a mixture, p-MWCNT + nanographite + nanonickel(II) oxide + nanoiron(II/III) oxide @Hb/Nf modified electrode and its 500 μM H_2O_2 electrocatalysis. Electrolyte is pH 7 PBS and ν = 10 mV/s.

modified electrode system. Finally, the low-cost i-MWCNT modified Hb electrode, GCE/i-MWCNT@Hb/Nf is subjected for the electrochemical investigation. As can be seen in part E of Figure 4, the electrode shows well-defined redox behavior at $E^{o\prime}$ = −0.38 V versus Ag/AgCl and the calculated Γ_{Hb} is 54.8(±1.1) × 10^{-10} mol/cm^2, which is 5.7 and 1.9 times higher than the i-SWCNT@Hb and p-MWCNT@Hb systems, respectively. Calculated peak-to-peak potential ($\Delta E_p = E_{pc} - E_{pa}$, E_{pc} = cathodic peak and E_{pa} = anodic peak potentials) is 79.0(±1) mV at ν = 50 mV/s and RSD for 10 continuous CV cycles is 0.8%. Although the $E^{o\prime}$ value is comparable with that of the Cat et al's reported value of −0.342 V versus SCE in pH 6.2 for the f-CNT-Hb-CTAB-Nf modified electrode,[25] the Γ_{Hb} value observed with GCE/i-MWCNT@Hb/Nf is 3577 times higher than their report. In addition, the above value is significantly higher over other recent reports viz., the EDC linker-f-CNT-Hb (9.3 times),[31] CNT-HA-Hb (5.8 times),[35] and ZnO-MWCNT-Hb-Nf (92 times)[44] hybrid CNT materials. Hence, it is clear that the Hb has enhanced electric wiring with i-MWCNT in this work. Possible reason/s for the observation is due to the embedded impurities; (i) metal oxides (Fe, Co, and Ni), and carbonaceous impurities such as (ii) amorphous and (iii) graphitic carbon materials.[37,45] These impurities may have some positive interaction with the Hb and help to connect significant amount of Hb units with i-MWCNT active sites and inturn to effective electron-transfer and H_2O_2 reduction characteristics. Note that carbon nanoparticulate systems such as C_{60}/cyclodextrin,[46a] graphitized mesoporous carbon,[46b] porous graphitized carbon monolith,[46c] and metal oxides like cobalt oxide nanoflower,[46d] Co_3O_4 nanoflakes,[46e] nanosized Fe_2O_3/acrylic acid copolymer,[46f] Fe_3O_4/Poly-(ethyleneimine),[46g] nickel oxide nanoparticles,[46h] as bulk materials, were reported for direct electron-transfer activity of Hb. To prove what kind of trace impurity has positive interaction with Hb, nanographite, amorphous carbon, and nanometal oxides of nickel(II) and iron (II/III) as models for the carbonaceous and metal oxides impurities of the i-MWCNT respectively were subjected to biosensor construction, as in the GCE/i-MWCNT@Hb/Nf case, discretely. If the impurities have some interaction with the Hb then appreciable electron-transfer and electrocatalytic behaviors could be obtained. In parts A–D of Figure 5, curve "a" shows typical CV responses of GCE/nanographite@Hb/Nf, GCE/nanonickel(II)oxide@Hb/Nf, GCE/nanoiron (II/III)oxide@Hb/Nf, and GCE/amorphous carbon@Hb/Nf modified electrodes in pH 7 PBS. Unfortunately, the above electrodes all showed highly irreversible or absence (for amorphous carbon) of CV peaks at −0.25 ± 0.1 V versus Ag/AgCl ($i_{pc}/i_{pa} \gg 1$). CV peak responses of the GCE/nanometallic oxide@Hb/Nf and GCE/carbonaceous@Hb/Nf electrodes are similar to the GCE/Hb/Nf and GCE/f-MWCNT@Hb/Nf as in parts A and B of Figure 4. Note that the stabilities of the graphite oxide@Hb/Nf and nanometal oxide@Hb/Nf working electrodes are better than the GCE/Hb/Nf (Figure S3 of the Supporting Information). To check whether the Hb is linked with the impurities of the MWCNT or not, H_2O_2 electrocatalytic reduction reactions were performed, as control experiments, with the above impurities/Hb modified electrodes (curve b in parts A–D of Figure 5). Detailed study for the H_2O_2 electrocatalytic reduction on the GCE/i-MWCNT@Hb/Nf is presented in section 3.4. As can be seen, the nanometal oxide@Hb/Nf and amorphous@Hb/Nf modified electrodes showed absence of any electrocatalytic signals (parts B–D of Figure 5); whereas significant H_2O_2 electrocatalytic-reduction peak current 16 (±1) μA and >100 mV overpotential with respect to the optimal electrode (section 3.4) were noticed with the graphite@Hb/Nf electrode (b in part A of Figure 5). Meanwhile, control unmodified impure metal oxides can also give H_2O_2 electrocatalytic signals at > −0.6 V versus Ag/AgCl (data not enclosed),[37a,b] which is 300 mV negative potential than that of the optimal Hb based biosensor electrode in pH 7 (section 3.4). From these results, it can be revealed that the

dx.doi.org/10.1021/jp3064933 | J. Phys. Chem. C 2012, 116, 23692–23703

carbonaceous impurity especially graphitic material has some positive interaction with the Hb and further to electrocatalytic H_2O_2 reduction, whereas the nanometal oxides, Fe_3O_4, NiO, and Co_3O_4, those were identified by the TGA and XRD analyses, may help to bind with the Hb units through complexation of amino and carboxyl groups from the Hb protein but are not helpful for any electron-transfer and H_2O_2 reduction reaction.

To support the graphite impurity interaction with Hb, a simulated i-MWCNT sample, which has been prepared using p-MWCNT with iron(II/III) oxide + nickel oxide + graphite (mixture of each of 1 mg/500 μL ethanolic solution), was subjected to Hb modification as in the optimal electrode preparation, and for H_2O_2 reduction reaction (part E of Figure 5). Observed CV behavior and H_2O_2 mediation response (16 ± 1 μA) are closer to the GCE/graphite@Hb/Nf system (part A of Figure 5). This observation undoubtfully supports the positive interaction by the graphite and absence of electron-transfer assistance by the metal oxide impurities in this work. Note that the simulated impurity modification procedure may result in attachment of the material on the outer surface of the p-MWCNT and not on the inner side as in the original i-MWCNT. Such a simulated configuration may block the uptake of Hb on multiwalls. Overall, multiwalled carbon unit along with graphite and metal oxide impurities as a whole is unique for enhanced Hb immobilization and efficient direct electron-transfer behavior in this work.

In continuation with the defined redox response, a feeble prepeak at −0.1 V versus Ag/AgCl was also noticed with the GCE/CNT@Hb/Nfs (CNTs = f-MWCNT, p-MWCNT, i-SWCNT, and i-MWCNT) at different extent (parts B−E of Figure 4); although the exact details for the reason are unclear now presumably due to energetically different CNT active sites and its interaction with the adsorbed Hb may be the cause for the prepeak. Note that similar observation was observed previously with anthraquinone adsorbed CNT modified electrodes.[47]

The amount of the Hb loading on i-MWCNT is calculated from EQCM measurements. Part F of Figure 4 is the typical open-circuit EQCM response of 0.19 cm^2 geometric area Au-EQCM/i-MWCNT working electrode (net amount of i-MWCNT on the Au-EQCM surface is 15 μg) exposed in 10 mg Hb dissolved 500 μL pH 7 PBS. A slight decrease in the mass change, $\Delta m = m - m(\text{ref})$ up to 10 s after that steep increase in the response was noticed. The initial mass decrease may be due to some equilibrium effect between the CNT and Hb. Calculated Hb mass at 1200 s (t = 20 min) of exposure time is 1.8 μg.

The effect of scan rate on the redox peak currents of the GCE/i-MWCNT@Hb/Nf was examined in pH 7 PBS (part A of Figure 6). A systematic increase in the peak current signals upon increase in the ν was observed. Plots of the anodic (i_{pa}) and cathodic (i_{pc}, as modulus values) peaks current values against scan rates were linear starting from the origin to 500 mV/s (part B of Figure 6). This observation suggests a surface confined electron-transfer behavior of the Hb-heme Fe(III)/Fe(II) units within the GCE/i-MWCNT@Hb/Nf system. It has been noticed that the i_{pc} values are slightly higher than the respective i_{pa} signals in part B of Figure 6, which might be due to some dissolved oxygen interference. Because the difference between the i_{pa} and i_{pc} current signals are small and constant, the i_{pc} values can be corrected with constant number easily.

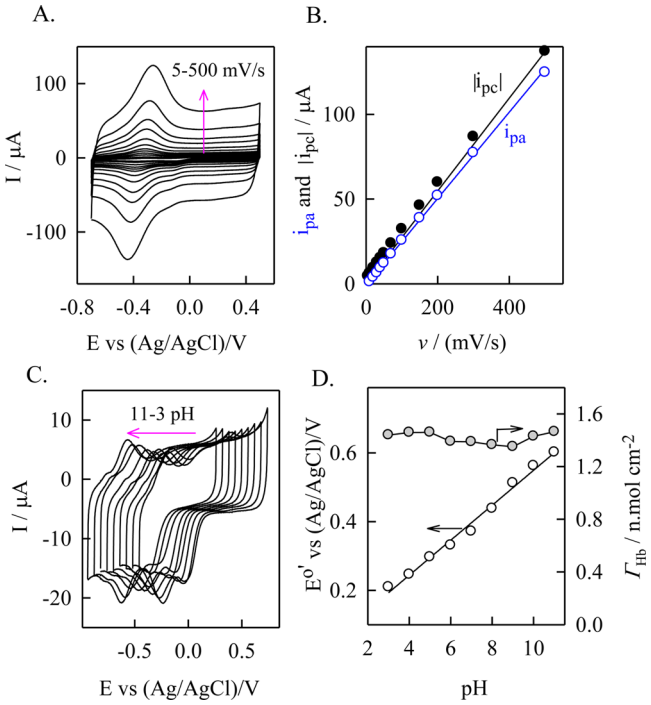

Figure 6. (A) Effect of scan rate (5−500 mV/s) on the CV of GCE/i-MWCNT@Hb/Nf in pH 7 PBS. (B) Plots of peak currents versus ν. (C) Effect of solution pH (3−11) on the CV response of GCE/i-MWCNT@Hb/Nf at a scan rate of 50 mV/s. (D) Plot of apparent standard electrode potential, $E^{o\prime}$ versus pH with slope, $S = dE^{o\prime}/dpH$ value of −50.9(±2) mV/pH and the corresponding linear equation is $E^{o\prime}/mV = -50.9(\pm 2)\ pH + 0.04(\pm 0.01)$, R = 0.9900.

Apparent heterogeneous electron-transfer rate constant, k_s and for the Hb-heme Fe(III)/Fe(II) redox within GCE/i-MWCNT@Hb/Nf was calculated by the Laviron model;[48]

$$\log(k_s/s^{-1}) = \alpha\log(1-\alpha) + (1-\alpha)\log\alpha - \log[(RT/\{nF(\nu/V.\ s^{-1})\})] - \alpha(1-\alpha)nF\Delta E_p/2.3RT \quad (-1)$$

In the above equation, α = transfer coefficient, n = number of transferred electrons per stoichiometric redox step, F = Faraday (C/mol), and other symbols have their own significance. On the basis of the relation, $E_{pc}/V = E^{o\prime} - (2.3RT/\alpha nF)\log(\nu/V.s^{-1})$, for a CV response of a thin film electron-transfer system[48] the factor α can be calculated from the slope ($2.3RT/\alpha nF$) of a plot of E_{pc} versus log ν (not shown). A slope, $S = dE/d\log\nu$ value of 0.058(±0.003) V was observed. By assuming n = 1, calculated α value is 0.5. The value implies symmetrical energy barrier for the electron-transfer of the Hb-heme Fe(III)/Fe(II) unit. Calculated heterogeneous electron-transfer rate constant, k_s = 0.98(±0.01) /s, by taking the ΔE_p value of 129(±1) mV at a ν = 200 mV/s. The value is comparable with that of the literature values viz., k_s = 1.25(±0.25) /s for the Hb-f-CNT-CTAB-Nf,[25] 0.84/s for the Hb-IL-MWCNT-CPE,[33] and 0.99/s for the Hb-polymer grafted f-MWCNT,[34] and it is better than the value of 0.05/s reported on the Hb-EDC linked-f-CNT.[31]

Next, effect of solution pH on the direct electron-transfer behavior of the GCE/i-MWCNT@Hb/Nf was examined by using CV measurements as in part C of Figure 6. Systematic shift in the peak potentials against the solution pH was

dx.doi.org/10.1021/jp3064933 | J. Phys. Chem. C 2012, 116, 23692−23703

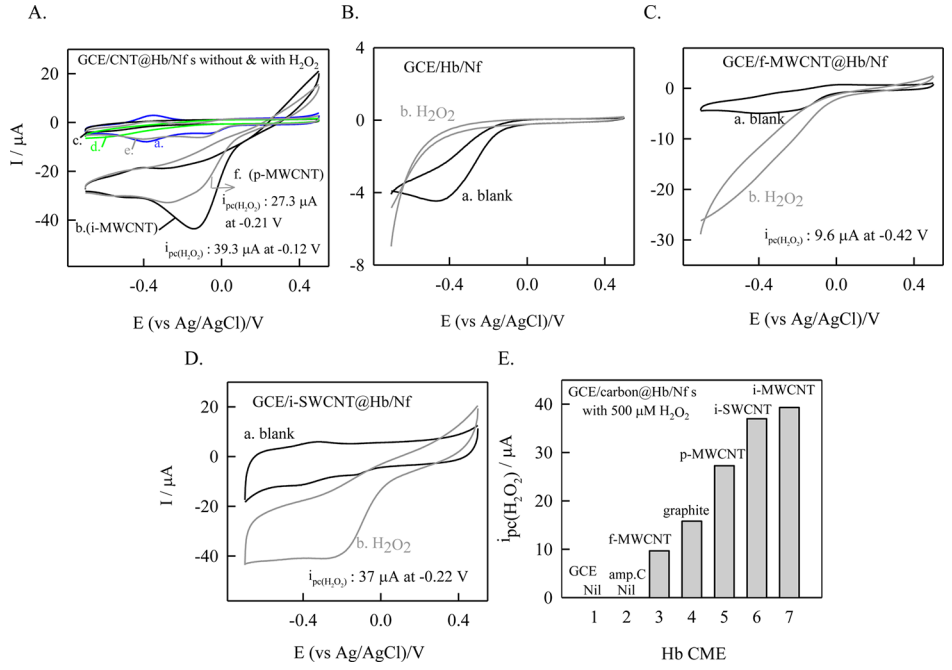

Figure 7. CV responses (A) GCE/i-MWCNT@Hb/Nf (a and b), GCE/i-MWCNT/Nf (c and d), and GCE/p-MWCNT@Hb/Nf (e and f) without (curves a, c, and e) with 500 μM H_2O_2 (curves b, d, and f), (B) GCE/Hb/Nf, (C) GCE/f-MWCNT@Hb/Nf, and (D) GCE/i-SWCNT@Hb/Nf in pH 7 PBS at ν = 10 mV/s. (E) Plot of $i_{pc(H_2O_2)}$ vs various Hb CMEs.

observed. Plot of $E^{o\prime}$ versus pH yielded a linear line with a slope, $S = dE^{o\prime}/dpH$ value of −50.9(±2) mV/pH, which is slightly lesser than the value of −58 mV/pH for the ideal Nernstian system, $E = E^{o} - 2.303(RT/F)pH$ involved with equal number of e^-/H^+ exchange reaction (part D of Figure 6). Such nonideal values were already been reported with the Hb-IL-CNT-CPE (−51 mV/pH),[33] Hb-polymer grafted MWCNT (−42 mV/pH),[34] and Hb-CNT-HA (−38 mV/pH) hybrid[35] electrodes. The reason for the nonideal value may be due to partial protonation of transligands and amino acids of the heme site. However, it also could indicate that a single protonation accompanies with one electron transfer of the Hb's redox process as: Hb-heme-Fe(III) + H^+ + e^- → Hb-heme-Fe(II). In addition to above, we also calculated Γ_{Hb} values from the net area under the CV redox peaks at different pH solutions (3−11) and the values were displayed as addition plot in part D of Figure 6. Interestingly, there is no significant alteration in the Γ_{Hb} even at acid and alkaline pHs, which indicates the compatibility and nondenaturation of the Hb in the GCE/i-MWCNT@Hb/Nf. Note that in the previous work serious Hb denaturation was noticed with conventional carbon based electrode in acid solution .[50]

3.4. Electrocatalytic Reduction of H_2O_2 on GCE/i-MWCNT@Hb/Nf. Electrocatalytic activity of the GCE/i-MWCNT@Hb/Nf was investigated with 500 μM of H_2O_2. Curve a of part A of Figure 7 is the CV response of the electrode GCE/i-MWCNT@Hb/Nf at ν = 10 mV/s in pH 7 PBS. In the presence of H_2O_2, marked cathodic peak at −0.12 V versus Ag/AgCl along with disappearance of the respective anodic peak was noticed (curve b in part A of Figure 7). The prepeak noticed at −0.1 V versus Ag/AgCl, due to the adsorption of Hb on energetically different i-MWCNT site, is responsible for the unusually low potential mediation of the H_2O_2 in this work. A control CV response of GCE/i-MWCNT/Nf with H_2O_2 yielded a cathodic reduction peak potential at −0.55 V versus Ag/AgCl (Figure 7(A)c and d), which is 350 mV higher overpotential than the GCE/i-MWCNT@Hb/Nf electrode. In continuation, the GCE/p-MWCNT@Hb/Nf was also subjected to H_2O_2 reduction experiment (e and f of part A of Figure 7). A shoulder-like response at −0.3 V versus Ag/AgCl and about half the time lower in the current response than the GCE/i-MWCNT@Hb/Nf electrode's H_2O_2 reduction was noticed. These observations indicate effective mediated reduction of the H_2O_2 by the i-MWCNT@Hb-heme Fe(III)/Fe(II) units-Nf hybrid in this work. Typical comparative electrocatalytic responses of different GCE/carbon@Hb/Nfs and its quantitative electrocatalytic current ($I_{pc(H_2O_2)}$, as a bar diagram) were given in parts B−E of Figure 7. Note that, although GCE/i-SWCNT@Hb/Nf yielded about 6 times lesser in the Γ_{Hb} value than the GCE/i-MWCNT@Hb/Nf, for the H_2O_2 mediation case the i-SWCNT electrode showed comparable mediation current (37 and 39 μA respectively for i-SWCNT and i-MWCNT modified electrodes (part E of Figure 7) along with 100 mV higher in overpotential. As can be revealed earlier, being rich in the graphite carbon impurity content (2.07 and 0.48% respectively with i-SWCNT and i-MWCNT, Table 1) played a key role for the overall enhancement of the H_2O_2 mediation with the GCE/i-SWCNT@Hb/Nf system.

The effect of H_2O_2 concentration [H_2O_2] on the CV of the GCE/i-MWCNT@Hb/Nf was examined (data not enclosed). The i_{pc} values linearly increased against increase in the [H_2O_2] up to 700 μM, after that a plateau in the response was noticed (Figure S4 of the Supporting Information). Calculated current sensitivity, as a slope (S) = $di_{pc}/d[H_2O_2]$ value normalized by scan rate (10 mV/s) and surface area (0.0707 cm^2) is 0.0283(±0.002) $A.M^{-1}.cm^{-2}.(mV/s)^{-1}$. This value is 3680 times higher over the previous report on the CNT@Hb modified pyrolytic graphite electrode sensitivity.[28]

3.5. Mechanism for the i-MWCNT@Hb/Nf Mediated H_2O_2 Reduction. Scheme 2 illustrates possible mechanism

dx.doi.org/10.1021/jp3064933 | J. Phys. Chem. C 2012, 116, 23692−23703

Scheme 2. Michaelis–Menten (MM) Reaction for the Electrocatalytic Reduction of H_2O_2 on GCE/i-MWCNT@Hb/Nf, rds = Rate Determining Step

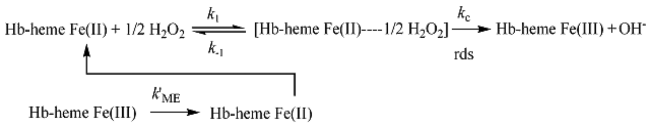

based on the Michaelis–Menten (MM) type reaction pathway for the selective electrocatalytic reduction of H_2O_2 by the Hb-heme Fe(III)/Fe(II) redox species with-in the GCE/i-MWCNT@Hb/Nf electrode.[38,51] Kinetic parameters, K_M = apparent MM rate constant ($(k_{-1} + k_c)/k_1$), k_c = first order chemical rate constant and k'_{ME} = heterogeneous modified electrode rate constant were calculated based on the standard MM equations,[38,51] and the values are; K_M = 2 mM, k_c = 2.27/s, and k'_{ME} = 3.03(±1.52) × 10^{-3} cm/s, respectively. Table 2 provides comparison of the k_s and K_M values with some of the literature reports. The K_M value of the present system is relatively higher than the other reported values (Table 2), which may indicate lower biocatalytic activity of the present electrode. However, stability and selectivity parameters are appreciably good, which enables excellent H_2O_2 real sample analysis further (sections 3.6 and 3.7).

3.6. Analytical Applications. Part A of Figure 8 shows comparison of typical amperometric *i*–*t* responses of GCE/i-MWCNT@Hb/Nf and GCE/i-MWCNT/Nf working electrodes for the continuous sensing of 50 μL spikes of the H_2O_2. As can be seen, marked increases in the H_2O_2 current signals were noticed only with the optimal electrode; whereas the Hb unmodified electrode GCE/i-MWCNT/Nf under the identical working condition showed nil signals. This observation supports electro-catalytic *reduction* of the H_2O_2 by the Hb heme-Fe(II)/Fe(III) active sites. Constructed calibration plot using the amperometric *i*–*t* data was linear in the window 50 to 300 μM with a current sensitivity and regression coefficient values of 8(±0.2) nA/μM (0.1131(±0.0028) A.M^{-1}.cm^{-2}) and 0.9949, respectively. Ten continuous spikes of 50 μM H_2O_2 results to an RSD value of 1.4%. Calculated detection limit (*S*/*N* = 3) for the H_2O_2 detection is 2.4 μM. The current sensitivity value obtained at 0 V versus Ag/AgCl in this work is comparable with the literature values (Table 2). Note that, ∼ −300 mV versus Ag/AgCl was often reported as detection potential for H_2O_2 biosensing in literature (Table 2). The current sensitivity can be improved further if the applied potential is moved toward more negative potentials in the present system.

The effect of interferences from various biochemicals such as cysteine (CySH), ascorbic acid (AA), uric acid (UA), nitrite (NO_2^-), and nitrate (NO_3^-) were examined on the working electrode at an applied potential of 0 V versus Ag/AgCl. As can be seen in part B of Figure 8, no marked alterations in the current signals were noticed upon the spikes of the above interfering biochemicals, which imply the selective H_2O_2 biosensing ability of the GCE/i-MWCNT@Hb electrode. It is surprising that the working electrode failed to show any current signal to nitrite, which is unusual because the Hb modified electrodes were reported to be effective for the nitrite reduction reaction too.[30,33] Possibly, the anionic nafion overlayer coating on the working electrode can ionically exclude the nitrite anion, and hence absence of any nitrite interference.

Pasteurized milks (#1 and #2), cosmetic bleach cream (#3, part C of Figure 8), and medical H_2O_2 (#4) samples were subjected to real-sample analysis by the standard addition method. Table S2 of the Supporting Information provides detailed information about the detected H_2O_2. After the dilution factor corrections, the corresponding H_2O_2 concentrations in those real samples are 18.4 (0.06%) and 430 mM (1.45%), respectively.

3.7. Stability and Reproducibility. Stability and reproducibility of the i-MWCNT@Hb/Nf composite were appreciably good. The SPCE/i-MWCNT@Hb/Nf matrix in pH 7 PBS was stable for 110 days if it is stored at RT or in the refrigerator (parts A and B of Figure S5 of the Supporting Information). Note that recent report based on functionalized carbon nanofiber–hemin (Heme B) modified electrode dipped in 0.2 M acetate buffer of pH 5.6 and stored at 4 °C and room temperature conditions showed 78% and 58% decreases in the current values respectively after 1 week of exposure time.[52] Finally, the reproducibility of the working electrode shows RSD value of 9.2% with respect to i_{pa} (data not enclosed). Manual preparation error is the possible reason for the slightly higher RSD over the expected value of 5%.

Table 2. Comparison of Electrochemical and Analytical Parameters (By Amperometric *i*–*t*) of Various Hb CMEs[a]

Hb CMEs	E° (mV)	Γ_{Hb} (× 10^{-10} mol.cm^{-2})	k_s (s^{-1})	k_M (mM)	D_L (μM) [E_{app} (mV)]	sensitivity (A.M^{-1}.cm^{-2})	linear range (μM)	ref
GCE/CMC–TiO_2–NTs@Hb	−340[c]				4.6 [−300]	0.183	4–64	17
GC/meso-Al_2O_3–PVA@Hb	−345[c]	1.2	3.17		0.02 [−250]	0.113	0.195–20.5	19
GCE/CSNs-CS@Hb	−325[c]	0.4	1.83		0.5 [−400]	0.014	0.75–216	24
PG/f-MWCNT@Hb	−360[c]	0.3				0.001	100–1300	28
GCE/Au-p-MWCNT/Hb@Hb	−370[c]			0.26	0.08 [−300]	0.112	0.2–3000	29
GCE/HA+f-MWCNT@Hb	−335[c]	9.3	5.05	0.007	0.09 [−380]	0.056	0.5–2	35
GCE/CM-DDAM@Hb	−184[b]	52.0	6.87	0.018	0.1 [−300]	0.328	0.1–60	46c
GCE/Co_3O_4–Nf@ Hb	−350[b]	3.1	2.9	0.136	0.1 [−230]	0.056	1–200	46e
GCE/NiO@Hb	−150[b]	0.17	5.2	1.37	0.6 [−300]	0.423	1–10	46h
GCE/i-MWCNT@Hb/Nf	−380[b]	54.8	0.98	2	2.4 [0]	0.113	50–500	this work

[a]CMC = Carboxymethyl cellulose; TiO_2–NTs = Titanium oxide Nanotubes; PVA = polyvinyl alcohol; CSNs = colloidal silver nanoparticles; CS = chitosan; PG = pyrolytic graphite; HA = hydroxyapatite; CM = carbon monolith; DDAM = didodecyl dimethyl ammonium bromide. [b]Vs Ag/AgCl. [c]Vs SCE and E_{app} = applied potential.

dx.doi.org/10.1021/jp3064933 | J. Phys. Chem. C 2012, 116, 23692–23703

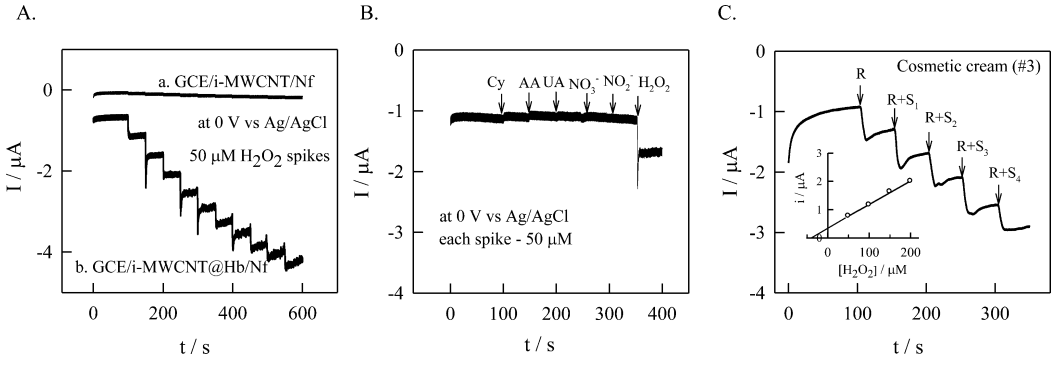

Figure 8. Amperometric i–t responses of (A) GCE/i-MWCNT/Nf (a) and GCE/i-MWCNT@Hb/Nf (b) for sensing of 50 μM spikes of H_2O_2, and (B) cysteine (CySH), ascorbic acid (AA), uric acid (UA), nitrate (NO_3^-), and nitrite (NO_2^-) successive sensing on a GCE/i-MWCNT@Hb/Nf in a stirred pH 7 PBS at an applied potential of 0 V vs Ag/AgCl. (C) Typical real H_2O_2 containing cosmetic real sample (R) by standard addition approach (R+S) and i vs $[H_2O_2]$ plot as an insert.

4. CONCLUSIONS

As commercially received impure-MWCNT was found to be a better material over the conventional functionalized-MWCNT and purified MWCNT, which requires extensive and time-consuming chemical treatments, for the electric wiring of the Hb along with nafion membrane on GCE. Graphite impurity, identified by TGA and XRD, were found to play a key role for the Hb direct-transfer reaction, whereas the metal oxide impurities assisted the binding of Hb on the i-MWCNT. No such facilitation was observed with amorphous carbon impurities. Qualitative electrochemical behavior of the Hb immobilized impure-MWCNT modified GCE (GCE/i-MWCNT@Hb/Nf) resembled the previous by reported Hb-based biosensors, which were constructed using functionalized CNT along with surfactant or several linkers based systems. Nevertheless, the Hb surface excess value (Γ_{Hb}), a parameter to determine the amount of immobilized Hb, was >3500 times higher than the standard literature report of Hb-surfactant-functionalized-CNT modified GCE. Only 40 minutes of working time is required to prepare the working biosensor. The new biosensor was highly selective for the sensing of hydrogen peroxide by amperometric method with up to the $[H_2O_2]$ = 300 μM at an applied operating potential of 0 V versus Ag/AgCl in pH 7 phosphate buffer solution. The i-MWCNT@Hb/Nf electrode was tolerable to ascorbic acid, cysteine, uric acid, and nitrate electrochemical signals too, unlike the conventional Hb based biosensor electrodes with electrocatalytic response to nitrite. The new biosensor developed in this work was useful to sense the hydrogen peroxide present in pasteurized milk, cosmetic bleaching cream, and medical samples. Because the approach is simple and of low cost, it can be extendable to prepare a hydrogen peroxide biosensor on disposable screen-printed electrode and further to hydrogen peroxide measuring device fabrication also.

■ ASSOCIATED CONTENT

Supporting Information

TGA responses of various carbon materials, AFM images, CV experiments on the stability of control sample modified electrodes, plot of $i_{pc(H_2O_2)}$ vs $[H_2O_2]$, and CV of long time stability of the SPCE/i-MWCNT@Hb/Nf, and comparative XRD data for the various carbon and control samples, and H_2O_2 containing cosmetic real sample analyses data. This material is available free of charge via the Internet at http://pubs.acs.org.

■ AUTHOR INFORMATION

Corresponding Author

*Fax: +91 416 2243092, tel: +91 −416- 2202754; e-mail: askumarchem@yahoo.com.

Notes

The authors declare no competing financial interest.

■ ACKNOWLEDGMENTS

The authors gratefully acknowledge Department of Science and Technology (DST), Nano Mission, India for the financial support. Authors also thank Dr. D. Sangeetha for her valuable support to this work.

■ REFERENCES

(1) Scheller, F. W.; Bistolas, N.; Liu, S.; Janchen, M.; Katterle, M.; Wollenberger, U. *Adv. Colloid Interface Sci.* **2005**, *116*, 111−120.
(2) Ardeleanu, I.; Margineanu, D. G.; Vais, H. *Bioelectrochem. Bioenerg.* **1983**, *11*, 273−277.
(3) Wu, Y.; Hu, S. *Microchim. Acta* **2007**, *159*, 1−17.
(4) Gundersen, S. I.; Chen, G.; Powell, H. M.; Palmer, A. F. *Biotechnol. Bioeng.* **2010**, *107*, 582−592.
(5) Jahr, J. S.; Lurie, F.; Driessen, B.; Tang, Z.; Louie, R. F.; Kost, G. *Am. J. Ther.* **2003**, *10*, 21−8.
(6) Campbell, M. K.; Farrell, S. O. *Biochemistry*, 5th ed.; Thomson Brooks/Cole Publisher: New Delhi, 2006.
(7) Chen, X. -H.; Ruan, C. -M.; Kong, J.-L.; Yang, R.; Deng, J. -Q. *Electroanalysis* **1998**, *10*, 695−699.
(8) Liu, H.; Wang, L.; Hu, N. *Electrochim. Acta* **2002**, *47*, 2515−2523.
(9) Li, J.; Zhou, L.; Han, X.; Liu, H. *Sens. Actuators, B* **2008**, *135*, 322−326.
(10) Liu, Y.; Wei, W. Z.; Liu, X. Y.; Zeng, X. -D.; Li, Y. -H.; Luo, S. -L. *Anal. Lett.* **2011**, *44*, 585−594.
(11) Ju, H.; Dong, L.; Chen, H. *Anal. Lett.* **1996**, *29*, 587−599.
(12) Sun, W.; Kong, J.; Deng, J. *Electroanalysis* **1997**, *9*, 115−119.
(13) Zhou, D. M.; Chen, H. Y. *Electroanalysis* **1997**, *9*, 399−402.
(14) Ye, J.; Baldwin, R. P. *Anal. Chem.* **1988**, *60*, 2263−2268.
(15) Zhang, Y. Z.; Zhao, H.; Yuan, Z. B. *Electroanalysis* **2002**, *14*, 382−386.
(16) Chen, J.; Stoecklein, W.; Scheller, F. W.; Wollenberger, U. *Anal. Lett.* **2003**, *36*, 2049−2059.
(17) Zheng, W.; Zheng, Y. F.; Jin, K. W.; Wang, N. *Talanta* **2008**, *74*, 1414−1419.
(18) Topoglidis, E.; Astuti, Y.; Duriaux, F.; Graetzel, M.; Durrant, J. R. *Langmuir* **2003**, *19*, 6894−6900.
(19) Yu, J.; Ma, J.; Zhao, F.; Zeng, B. *Electrochim. Acta* **2007**, *53*, 1995−2001.
(20) Pan, Z. Q.; Fan, H.; Shi, C. -G.; Bao, N.; Yu, C. M.; Gu, H. Y. *Microchim. Acta* **2011**, *173*, 277−283.

(21) Li, Y.; Zhang, Q.; Li, J. *Talanta* **2010**, *83*, 162−166.
(22) Zhou, Y.; Li, Z.; Hu, N.; Zeng, Y.; Rusling, J. F. *Langmuir* **2002**, *18*, 8573−8579.
(23) Han, X.; Cheng, W.; Zhang, Z.; Dong, S.; Wang, E. *Biochim. Biophys. Acta, Bioenerg.* **2002**, *1556*, 273−277.
(24) Yu, C.; Zhou, X.; Gu, H. *Electrochim. Acta* **2010**, *55*, 8738−8743.
(25) Cai, C.; Chen, J. *Anal. Biochem.* **2004**, *325*, 285−292.
(26) Feng, X.; Li, R.; Hu, C.; Hou, W. *J. Electroanal. Chem.* **2011**, *657*, 28−33.
(27) Yang, P.; Zhao, Q.; Gu, Z.; Zhuang, Q. *Electroanalysis* **2004**, *16*, 97−100.
(28) Zhao, L.; Liu, H.; Hu, N. *J. Colloid Interface Sci.* **2006**, *296*, 204−211.
(29) Chen, S.; Yuan, R.; Chai, Y.; Zhang, L.; Wang, N.; Li, X. *Biosens. Bioelectron.* **2007**, *22*, 1268−1274.
(30) Zhang, L.; Yi, M. *Bioprocess Biosyst. Eng.* **2009**, *32*, 485−492.
(31) Zhang, R.; Wang, X.; Shiu, K. K. *J. Colloid Interface Sci.* **2007**, *316*, 517−522.
(32) Zhang, X.; Qi, B.; Zhang, S. *Anal. Lett.* **2008**, *41*, 3100−3112.
(33) Wei, W.; Jin, H. H.; Zhao, G. C. *Microchim. Acta* **2009**, *164*, 167−171.
(34) Wen, Y.; Wu, H.; Chen, S.; Lu, Y.; Shen, H.; Jia, N. *Electrochem. Acta* **2009**, *54*, 7078−7084.
(35) Zhao, H. Y.; Xu, X. X.; Zhang, J. X.; Zheng, W.; Zheng, Y. F. *Bioelectrochem* **2010**, *78*, 124−129.
(36) Shie, J. W.; Yogeswaran, U.; Chem, S. M. *Talanta* **2009**, *78*, 896−902.
(37) (a) Banks, C. E.; Crossley, A.; Salter, C.; Wilkins, S. J.; Compton, R. G. *Angew. Chem., Int. Ed.* **2006**, *45*, 2528−2533. (b) Sljukic, B.; Banks, C. E.; Compton, R. G. *Nano Lett.* **2006**, *6*, 1556−1558. (c) Pumera, M.; Miyahara, Y. *Nanoscale* **2009**, *1*, 260−265. (d) Pumera, M.; Iwai, H. *Chem. Asian J.* **2009**, *4*, 554−560. (e) Pumera, M. *J. Phys. Chem. C* **2009**, *113*, 4401−4405. (f) Ambrosi, A.; Pumera, M. *Chem.—Eur. J.* **2010**, *16*, 10946−10949. (g) Stuart, E J. E.; Pumera, M. *Chem.—Eur. J.* **2011**, *17*, 5544−5548. (h) Stuart, E. J. E.; Pumera, M. *J. Phys. Chem. C* **2011**, *115*, 5530−5534. (i) Chng, E. L. K.; Pumera, M. *Chem.—Eur. J.* **2012**, *18*, 1401−1407. (j) Ambrosi, A.; Pumera, M. *J. Phys. Chem. C* **2011**, *115*, 25281−25284.
(38) Kumar, A. S.; Barathi, P.; Pillai, K. C. *J. Electroanal. Chem.* **2011**, *654*, 85−95.
(39) Banks, C. E.; Crossley, A.; Salter, C.; Wilkins, S. J.; Compton, R. G. *Angew. Chem., Int. Ed.* **2006**, *45*, 2533−2537.
(40) Kitamura, H.; Sekido, S.; Takeuchi, H.; Ohno., M. *Carbon* **2011**, *49*, 3851; *Carbon* **2011**, *49*, 3851−3856.
(41) (a) Hou, P. -X.; Liu, C.; Cheng, H. -M. *Carbon* **2008**, *46*, 2003−2025. (b) Moraitis, G.; Spitalsky, Z.; Ravani, F.; Siokou, A.; Galiotis, C. *Carbon* **2011**, *49*, 2702−2708. (c) Reyhania, A.; Mortazavib, S. Z.; Nozad Golikandb, A.; Moshfegha, A. Z.; Mirershadi, S. *J. Power Sources* **2008**, *183*, 539−543. (d) Jeong, H. -K.; Lee, Y. P.; Jin, M. H.; Kim, E. S.; Bae, J. J.; Lee, Y. H. *Chem. Phys. Lett.* **2009**, *470*, 255−258. (e) Pumera, M. *Langmuir* **2007**, *23*, 6453−6458. (f) Downs, R. T.; Hill-Wallace, M. *Am. Mineral.* **2003**, *88*, 247−250. (g) Cairns, R. W.; Ott, E. *J. Am. Chem.* **1933**, *55*, 527−533.
(42) (a) Charradi, K.; Forano, C.; Prevot, V.; Madern, D.; Amara, A. B. H.; Mousty, C. *Langmuir* **2010**, *26*, 9997−1004. (b) Wang, M.; Zhengz, J. *J. Electrochem. Soc.* **2012**, *159*, 150−156.
(43) Kumar, A. S.; Swetha, P. *J. Electroanal. Chem.* **2010**, *642*, 135−142.
(44) Ma, W.; Tian, D. *Bioelectrochem.* **2010**, *78*, 106−112.
(45) Ji, X.; Kadara, R. O.; Krussm, J.; Chen, Q.; Banks, C. E. *Electroanalysis* **2010**, *22*, 7−19.
(46) (a) Li, M -X.; Li, N -Q.; Gu, Z -N.; Zhou, X -H.; Sun, Y -L.; Wu, Y -Q. *Anal. Chim. Acta* **1997**, *356*, 225−229. (b) Lu, X.; Xiao, Y.; Lei, Z.; Chen, J.; Zhang, H.; Ni, Y.; Zhang, Q. *J. Mater. Chem.* **2009**, *19*, 4707−4714. (c) He, X.; Zhou, L.; Nesterenko, E. P.; Nesterenko, P. N.; Paull, B.; Omamogho, J. O.; Glennon, J. D.; Luong, J. H. T. *Anal. Chem.* **2012**, *84*, 2351−2357. (d) Zhu, Z.; Li, X.; Zeng, Y.; Sun, W.; Zhu, W.; Huang, X. *J. Phys. Chem. C* **2011**, *115*, 12547−12553. (e) Lu, X.; Zou, G.; Li, J. *J. Mater. Chem.* **2007**, *17*, 1427−1432. (f) Gong, J.; Lin, X. *Microchem. J.* **2003**, *75*, 51−57. (g) Cao, D.; Hu, N. *Biophys. Chem.* **2006**, *121*, 209−217. (h) Salimi, A.; Sharifi, E.; Noorbakhsh, A.; Soltanian, S. *Electrochem. Commun.* **2006**, *8*, 1499−1508.
(47) Kumar, A. S.; Swetha, P. *Colloids Surf., A* **2011**, *384*, 597−604.
(48) Laviron, E.; Roullier, L. *J. Electroanal. Chem.* **1980**, *115*, 65−74.
(49) Sun, W.; Zhai, Z.; Wang, D.; Liu, S.; Jiao, K. *Bioelectrochem.* **2009**, *74*, 295−300.
(50) Sun, W.; Gao, R.; Jiao, K. *J. Phys. Chem. B* **2007**, *111*, 4560−4567.
(51) Lyons, M. E. G.; Fitzgerald, C. A.; Smyth, M. R. *Analyst* **1994**, *119*, 855−861.
(52) Valentini, F.; Cristofanelli, L.; Carbone, M.; Palleschi, G. *Electrochim. Acta* **2012**, *63*, 37−46.